IOP PUBLISHING BIOMEDICAL MATERIALS

Biomed. Mater. **7** (2012) 065006 (11pp) doi:10.1088/1748-6041/7/6/065006

Impregnation of silver sulfadiazine into bacterial cellulose for antimicrobial and biocompatible wound dressing

Jiabin Luan[1,3], **Jian Wu**[1,3], **Yudong Zheng**[1,4], **Wenhui Song**[2], **Guojie Wang**[1], **Jia Guo**[1] **and Xun Ding**[1]

[1] School of Materials Science and Engineering, University of Science and Technology Beijing, Beijing 100083, People's Republic of China
[2] Wolfson Center for Materials Processing, School of Engineering and Design, Brunel University, London UB8 3PH, UK

E-mail: zhengyudong@mater.ustb.edu.cn

Received 5 July 2012
Accepted for publication 6 November 2012
Published 26 November 2012
Online at stacks.iop.org/BMM/7/065006

Abstract

Silver sulfadiazine (SSD) is a useful antimicrobial agent for wound treatment. However, recent findings indicate that conventional SSD cream has several drawbacks for use in treatments. Bacterial cellulose (BC) is a promising material for wound dressing due to its outstanding properties of holding water, strength and degradability. Unfortunately, BC itself exhibits no antimicrobial activity. A combination of SSD and BC is envisaged to form a new class of wound dressing with both antimicrobial activity and biocompatibility, which has not been reported to date. To achieve antimicrobial activity, SSD particles were impregnated into BC by immersing BC into SSD suspension after ultrasonication, namely SSD–BC. Parameters influencing SSD–BC impregnation were systematically studied. Optimized conditions of sonication time for no less than 90 min and the proper pH value between 6.6 and 9.0 were suggested. The absorption of SSD onto the BC nanofibrous network was revealed by XRD and SEM analyses. The SSD–BC membranes exhibited significant antimicrobial activities against *Pseudomonas aeruginosa*, *Escherichia coli* and *Staphylococcus aureus* evaluated by the disc diffusion method. In addition, the favorable biocompatibility of SSD–BC was verified by MTT colorimetry, epidermal cell counting method and optical microscopy. The results demonstrate the potential of SSD–BC membranes as a new class of antimicrobial and biocompatible wound dressing.

(Some figures may appear in colour only in the online journal)

1. Introduction

Infection is one of the most frequent complications in the wound-healing process. Infection control is very important not only in the prevention of secondary infection, but also in maintaining a proper wound healing process [1]. Besides, infections caused by bacteria usually result in exudation around the wound site [2]. Improved wound dressings that provide an inherent antimicrobial effect by eluting germicidal compounds have been developed to respond to the problems associated with conventional topical treatments using ointments and creams [3]. Hydrogels, hydrocolloids, films, gauzes, alginates, biologics and foams are among the many classes of dressings available to healthcare professionals [4]. Wound dressings help maintain the proper moisture level and constant temperature of the wound bed, accelerate healing, activate autolytic debridement of the wound, protect newly formed cells, facilitate angiogenesis and re-epithelization,

[3] These authors contributed equally to this work.
[4] Author to whom any correspondence should be addressed.

alleviate pain and protect the wound against bacteria and contamination [5].

Bacterial cellulose (BC) is a kind of extra cellular polysaccharide produced by several bacteria, such as *Acetobacter xylinum,* the genus *Gluconoacetobacter, Sarcina,* etc, into long non-aggregated nanofibrils [6, 7]. BC was used traditionally in the food industry [8, 9], later in the fabrication of reinforced paper [10]. Recently, it was investigated as a material for medical applications e.g. cartilage scaffolds [11, 12], wound dressings [5, 13], dental implants [14–16], nerve regeneration [17], vascular grafts [17–20] and drug delivery systems [21, 22]. Regardless of the identical chemical composition, the mechanical properties and microstructure of BC differ from those of vegetable cellulose (VC). BC possesses higher tensile strength and modulus, higher water-holding capacity, higher crystallinity and a finer fibril network [23, 24]. Besides, owing to its fibril network structure similar to the extracellular matrix of human skin, BC is under investigation as a potential skin substitute in treating extensive burns. The never-dried cellulose membrane is a highly nano-porous material that allows for the potential transfer of antibiotics or other medicines into the wound, meanwhile serving as an efficient physical barrier against any external infection [25]. Other advantages of BC as a wound dressing have been reported, in that it can control wound exudates and provide a moist environment to a wound, resulting in better wound healing [5]. However, BC itself has no antimicrobial activity and cannot prevent wound infection, which is a major factor common to all wound care, especially the burn wounds, traumatic injuries and surgical procedures [26]. To date, researchers have researched different systems with BC for wound dressing applications: BC–Ag nanocomposites (*in situ* synthesis) [5, 24, 27], BC dry films containing benzalkonium chloride (simple impregnation) [28], BC–AgCl membranes (*in situ* synthesis) [29], BC/chitosan, BC/PEG and BC/gelatin composites (simple impregnation) [30].

The gold standard in topical burn treatment is silver sulfadiazine (SSD), which is most commonly deployed for partial- and full-thickness burns [31, 32]. Among antimicrobial agents, SSD is a broad spectrum antimicrobial agent that controls yeasts, molds, other types of fungi, and bacteria, typically including: *Pseudomonas aeruginosa*, *Escherichia coli* as well as *Staphylococcus aureus* [33, 34]. SSD readily ionizes to release silver ions, which intercalate into the microbial DNA forming a relatively strong bonding. Sulfadiazine interferes with many cellular metabolic processes, including DNA synthesis, folic acid pathways and the respiratory electron transport system, and can also interact with thiol groups on microbial proteins [35, 36]. Traditionally, SSD is applied with cream which causes several drawbacks in the treatment. Increased inflammation observed with SSD is caused by the water soluble cream base itself [31]. The hydrophobicity of the cream base tends to form an adhesive pseudo-eschar which is difficult to distinguish from a burn eschar and inhibits the penetration of SSD into burn wounds [37–40]. Clinically, the drainage of the exudates is also very important, especially in the management of severe burns where necrotic tissue is present, since an accumulation of the exudates beneath the dressing promotes bacterial growth [41]. Unfortunately, the SSD cream itself cannot absorb the exudates.

In the above context, we hypothesize that the association of SSD organic complex with biopolymers such as BC may represent an interesting approach to developing new antimicrobial biomaterials which may overcome the shortcomings of current wound dressings and also find a variety of other applications. To our knowledge, SSD–BC membranes have not been used or investigated for antimicrobial wound dressing applications. Although researchers have contributed a lot to reveal the singular properties of BC and its composites with antimicrobial activity, the cytocompatibility of these antimicrobial composites such as BC–Ag, BC–benzalkonium chloride and BC–AgCl have not been reported [5, 24, 27–30]. The aim of this work is to testify this hypothesis by developing SSD impregnated BC and understanding the antimicrobial and biocompatible properties of SSD–BC.

We put forward an ultrasonication-assisted impregnation method of introducing SSD particles into BC nanofibrous network. To achieve good antimicrobial properties, a range of conditions of impregnating SSD complex with BC were performed and optimized, e.g. ultrasonication time, pH value of the environment as well as the zeta potential of BC and SSD. XRD and SEM techniques were applied to reveal the structure and morphology of SSD–BC after the impregnation. The antibacterial activity of SSD–BC membranes in the presence of *P. aeruginosa*, *E. coli* and *S. aureus* were characterized. The favorable biocompatibility of SSD–BC was verified by MTT colorimetry, epidermal cell counting method as well as optical microscopy.

2. Materials and methods

2.1. Preparation and purification of BC membranes

BC membranes were purchased from Hainan Yida Food Co. Ltd (China). Deionized water was used to flush the BC membranes several times to remove culture solution and impurities on the surface. Then the membranes were immersed in NaOH solution (0.1 M, Beijing Reagent Factory) maintained at 90 °C for an hour in a thermostatic water bath to get rid of the biomass and residual culture medium in the pellicles. Subsequently, the membranes were thoroughly rinsed with deionized water until the pH of the washing liquid was neutral and finally immersed in deionized water prior to use.

2.2. Impregnation of SSD into BC membranes

SSD content of 1–2 wt% has been shown to have excellent anti-bacterial and anti-inflammatory effects on wounds. This may explain the fact that the concentration of SSD in the products on the market is in the similar range. In this work, 2 wt% SSD–water suspension (pH = 7.0, Yancheng Cunyi Chemical Co. Ltd, China) was also prepared. Before impregnating SSD with BC, proper conditions were studied as follows.

2.2.1. Ultrasonication. To acquire more homogeneous particles in size, 2 wt% SSD suspension (pH = 7.0) was firstly stirred by a SZCL magnetic stirrer (YUHUA®, China) for 1 d. SSD suspension was then ultrasonicated by a SCIENTZ® JY92-II,Ultrasonic Cell Pulverizer (China) for different periods of time to achieve SSD particles with various diameters. The diameter of SSD particles was determined using a Delsa™ Nano C Particle Analyzer (Beckman Coulter®, USA). The particle size of each sample was measured three times, and the measurement results were analyzed in terms of mean diameter ± standard deviation. In addition, the morphology of SSD particles was assessed by an Optec BK300 Optical Microscope (China).

2.2.2. pH value. The groups of SSD suspension sonicated for 90 min were selected for study on the effect of different pH environments. HCl solution was applied to adjust the solution to be acidic with pH = 5, 3 and 1; NaOH solution was applied to adjust the solution to be alkaline with pH = 9, 11 and 13. After 6 h, the particle diameter of each sample (including the original pH = 7.0 sample) was measured using the same particle analyzer described above.

2.2.3. Zeta potential. Zeta potential of SSD particles sonicated for different periods of time was measured in an aqueous medium. In addition, the zeta potential of the group sonicated for 90 min was analyzed in different pH solutions along with BC. All these experiments were also carried out using the Delsa™ Nano C Particle Analyzer (Beckman Coulter®, USA).

To find out the proper impregnation conditions, SSD particles were impregnated into BC membranes by immersing BC pellicles into SSD suspension which had been sonicated at pH = 8.0 for different periods of time, up to 24 h. The proportion of BC mass/SSD suspension volume is approximately 2/7 (g mL^{-1}). Following this, samples were sealed from light and kept at 4 °C in a refrigerator for future use. The amount of SSD particles impregnated into BC was quantified by an atomic absorption spectrometer (AAS) (Beijing, Beijing Kechuang Haiguang Instrument Co., Ltd, GGX-600). Samples were dissolved in 98% sulfuric acid and then diluted with deionized water to 20 times their original volume. The Ag content in the solution was measured by AAS and the SSD content in the sample was calculated according to the percentage of Ag in SSD as follows:

$$m_{\mathrm{SSD}} = \frac{\rho_{\mathrm{Ag}} V}{S} \times 100 \div \left(\frac{M_{\mathrm{Ag}}}{M_{\mathrm{SSD}}}\right) = 19.96\rho_{\mathrm{Ag}}, \qquad (1)$$

where m_{SSD} is the amount of SSD particles (mg/100 cm^2) impregnated in BC, ρ_{Ag} is the mass concentration of Ag (μg mL^{-1}) in the solution measured by AAS, V is the volume of the solution (mL), S is the area of BC sample (cm^2), M_{Ag} is the relative atomic mass of Ag and M_{SSD} is the relative molecular mass of SSD.

2.3. Characterization

2.3.1. X-ray diffraction. X-ray diffraction (XRD) tests of pure BC, SSD and SSD–BCs (all samples were freeze-dried at −40 to −50 °C) sonicated for different periods of time were performed using a Rigaku D/max-RB x-ray diffractometer (Japan) with a thin pellicle attachment. The samples were placed in the sample holder and scanned at a rate of 9° min^{-1} from 5° to 80° (2θ).

2.3.2. Scanning electron microscopy. Samples of BC and SSD–BCs were freeze-dried (−40 to −50 °C) to constant weight before being examined by scanning electron microscopy (SEM). For improved contrast, the specimens were sputtered with a thin layer of evaporated gold. The morphology of BC and SSD–BC was observed by an Apollo 300 scanning electron microscope (UK) equipped with an electron optical system with a 10 keV capacity electron gun and an electron detector. Elemental maps of the composite in BC were obtained using an energy dispersive spectrometer (EDS, Oxford, INCA).

2.4. Assay of antimicrobial activity

Antibacterial activity of the SSD–BCs was determined for *P. aeruginosa* (ATCC10211), *E. coli* (ATCC44113) and *S. aureus* (ATCC26085) using the disc diffusion method (AATCC-90). Initial cultures of these strains were prepared by incubating at 37 °C for 24 h: *Staphylococcus* medium for *S. aureus*; eosin-methylene blue medium for *E. coli*; blood agar medium for *P. aeruginosa*. After that, the cultures were appropriately diluted to the density of 1×10^5 cm^{-2} by sterile saline solution. Subsequently, BC (control sample) and SSD–BC discs with uniform size (6.5 mm diameter) were placed on the bacteria-seeded agar plates (8 per plate) and cultured in an incubator at 37 °C for 24 h. The inhibition zone was estimated by measuring the diameter of the nearest whole millimeter of the inhibited growth around the sample disc and was performed in triplicates.

2.5. Assay of biocompatibility

2.5.1. Cell culture. Westar fetal rat epidermal cells (Experimental Animal Center of Military Medical Sciences, China) were incubated in 2 mL Dulbecco's modified Eagle's medium (DMEM) supplemented with 10% fetal bovine serum (FBS) (GIBCO). Samples of SSD–BC discs were prepared by soaking in SSD suspension sonicated for different periods of time over 24 h and were then cut into 15 mm diameter to fit 24-well cell culture polystyrene plates. Before usage, the membranes were sterilized by γ-irradiation. The BC and SSD–BC samples were placed in 24-well cell culture polystyrene plates seeded with 1 mL Westar fetal rat epidermal cells (1×10^4 mL^{-1}) per disc and cultured in 5% CO_2 at 37 °C for 1 d, 4 d, 7 d and 10 d. The culture medium was changed on the fourth and seventh day.

2.5.2. Cell morphology observation. To observe cell morphology and distribution, epidermal cells cultured for 1 d, 4 d, 7 d and 10 d were observed, using a Leica DMI 4000 semi-automatic inverted biological microscope (Germany).

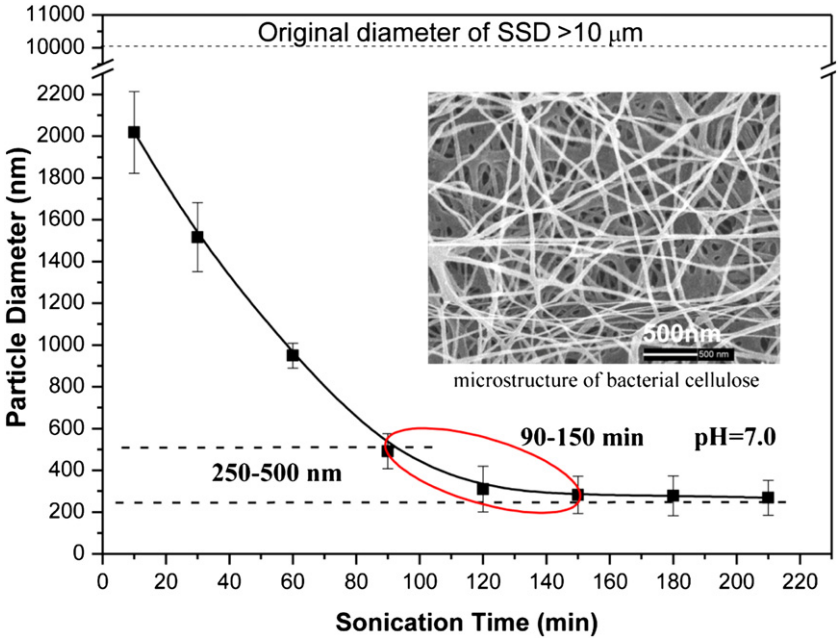

Figure 1. The curve of 2% SSD particle diameter versus sonication time. The inset is a SEM image of original bacterial cellulose.

2.5.3. Cell proliferation assay. Cells cultured in wells without membranes served as controls in this study. To investigate cell proliferation effect, epidermal cells were counted with a hemocytometer at 1 d, 4 d, 7 d and 10 d. The nutrient solution was removed and then cells were detached with 0.5 mL 0.25% Trypsin-0.02% EDTA (SCIENTIFIC RESEARCH SPECIAL). 10 min later, 0.5 mL DMEM–FBS was added to end cell digesting. The number of cells in suspension was counted with a hemocytometer. MTT assay was carried out at 1 d, 4 d, 7 d and 10 d. 100 μL of MTT solution (5 mg mL^{-1}) was added to each well and incubated for 4 h at 37 °C. Mitochondrial dehydrogenases of viable cells selectively cleaved the tetrazolium ring, yielding blue/purple formazan crystals. The medium was then replaced with 500 μL of DMSO to completely dissolve the MTT crystals formed previously by shaking homogeneously for about 10 min. Solubilized formazan products were quantified by spectrophotometry at 570 nm using a UNICO^{TM} WFZ UV-2100 Spectrophotometer (China).

2.6. Statistical analysis

All experiments were repeated at least three times with the number of antimicrobial and biocompatible assay samples: $n = 8$. Data are presented as means $\pm$ standard deviation. The statistical assay was performed using Student's *t*-test and the differences were considered statistically significant at $P < 0.05$.

3. Results and discussion

3.1. Parameters influencing SSD–BC impregnation

3.1.1. Particle diameter. Particle diameter of SSD decreased as the sonication time increased and then reached a stable value around 300 nm after sonicating for 120 min, at pH = 7.0 (figure 1). A SEM image of an original BC inset in figure 1 shows the unique three-dimensional fibrous structure of BC, with average pore size around 500 nm. Thus, to impregnate SSD into the network of BC, the optimized sonication time between 90 and 150 min was chosen, in which case the particle diameter was in a range from 250 to 500 nm. Otherwise, SSD particles would be too large to permeate through the fibrous network of BC.

With increasing sonication time, the morphology of SSD particles became more regular and uniform (figure 2). It is important to note that particles sonicated for 90 min became approximately spherical in shape. Such spherical morphology is envisaged to make the diffusion, permeation and impregnation of SSD easier. Therefore, the sonication time is recommended to be at least 90 min.

The influence of pH value on SSD particle diameter was then studied under the condition of sonication for 90 min. Figure 3 shows a series of photos of SSD suspension under different pH environments (standing for 6 h). Results indicated that pH had a great impact on the particle diameter of SSD. SSD particles appeared to agglomerate and precipitate easily when pH was either 1 or 13, in which case particle diameter was 3 μm on average. This may be due to precipitation reactions in different conditions. When HCl (pH = 1 or 3) was added into SSD suspension, Ag^+ could react with Cl^- to form AgCl ($[Ag^+][Cl^-] > K_{sp}(AgCl)$). In the case of pH = 13, strong basicity offered enough OH^- to react with Ag^+ to generate Ag_2O. Either AgCl or Ag_2O precipitates were suspected to result in a larger particle diameter in the suspension. Obviously, SSD suspension could not be easily impregnated into BC under strongly acidic and alkaline conditions for the reason that SSD particles were unstable and too large to get into the pores of BC. Hence, pH value between 5.0 and 9.0 was considered

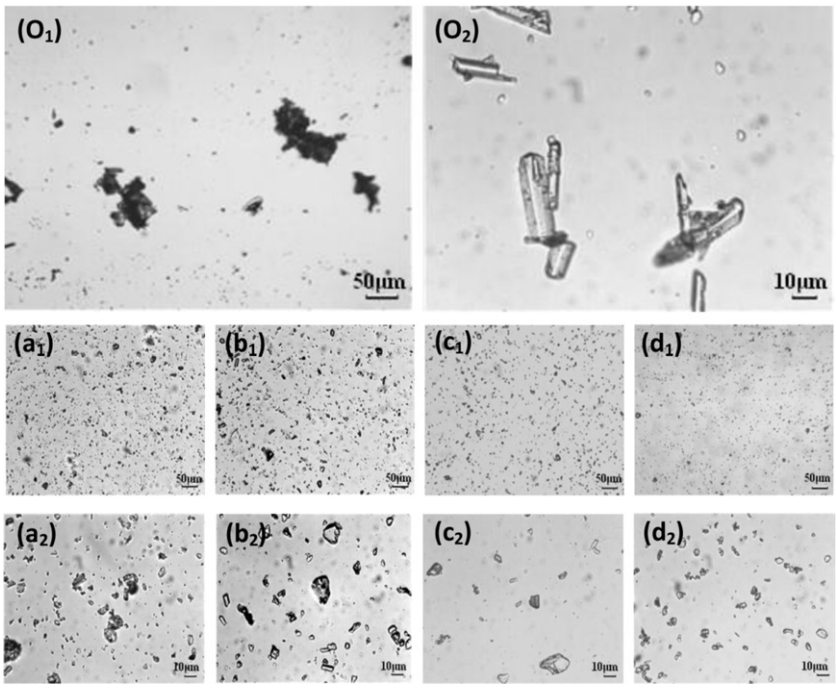

Figure 2. Optical microscopic images of 2% SSD particles of different sonication time: (O_1)(O_2) 0 min; (a_1)(a_2) 10 min; (b_1)(b_2) 30 min; (c_1)(c_2) 60 min; (d_1)(d_2) 90 min.

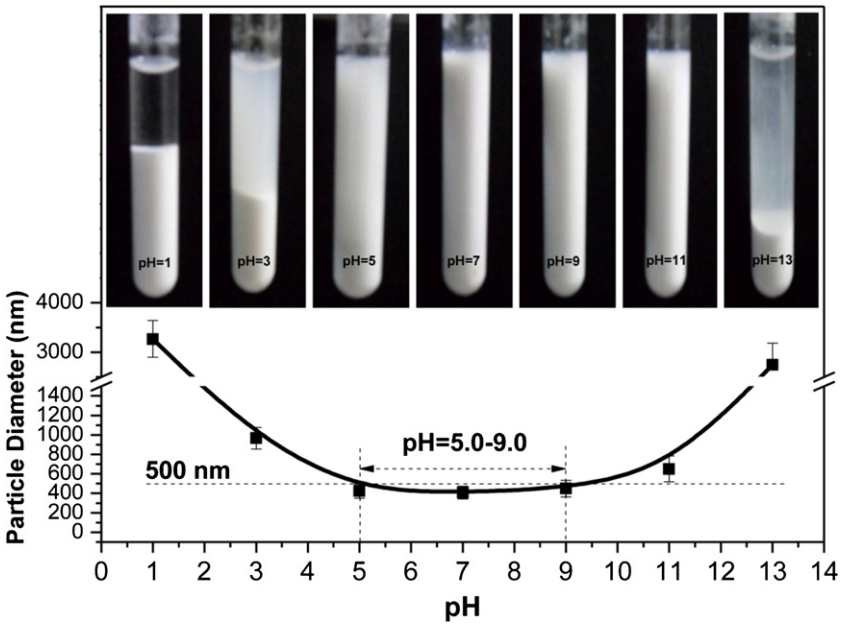

Figure 3. The curve of 2% SSD (sonicated for 90 min) particle diameter versus pH value.

optimum, under which circumstance SSD particle diameter was 500 nm on average.

3.1.2. Zeta potential. BC possessed weakly positive surface charges since its zeta potential was measured to be merely 0.24 mV. Its zeta potential kept consistent despite the change of pH value as shown in figure 4(*a*). At a fixed pH condition (pH = 7.0 in figure 4), the negative zeta potential of SSD particles remained more or less unchanged during different periods of sonication as shown in figure 4(*b*). On the other hand, the surface charges of SSD particles were under the control of the solution condition. The strong influence of pH value was clearly evident on the dramatic changes of the zeta potential of SSD particles from positive to negative and then back to positive in the range of pH from 1 to 13 (figure 4(*c*)). Notably, SSD's zeta potential reached the most negative value of –46 mV at pH $\approx$ 9.7. As a consequence, electrostatic interaction [42] developed between the negatively charged

Table 1. Impregnation conditions and relevant data (2% SSD, pH = 8.0).

Groups	Samples	pH	Sonication time of SSD Particles (min)	Diameter of particles (nm)	SSD content (mg/100 cm^2)
C0	BC	8.0	—	—	0
S0	BC + SSD	8.0	0	>10 μm	10.10 ± 1.86
S1	BC + SSD	8.0	90	491.3 ± 84.3	15.35 ± 3.10
S2	BC + SSD	8.0	120	310.2 ± 109.7	20.24 ± 1.72
S3	BC + SSD	8.0	150	282.3 ± 9.2	23.60 ± 2.54

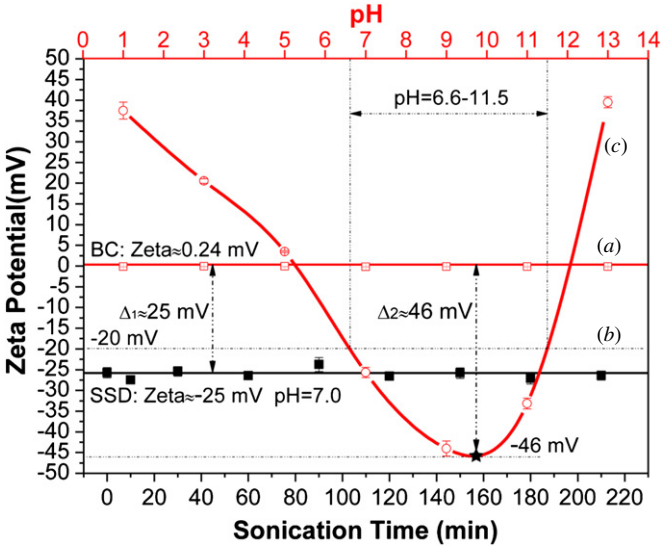

Figure 4. (*a*) BC zeta potential versus pH; (*b*) 2% SSD zeta potential versus sonication time; (*c*) 2% SSD (sonicated for 90 min) zeta potential versus pH.

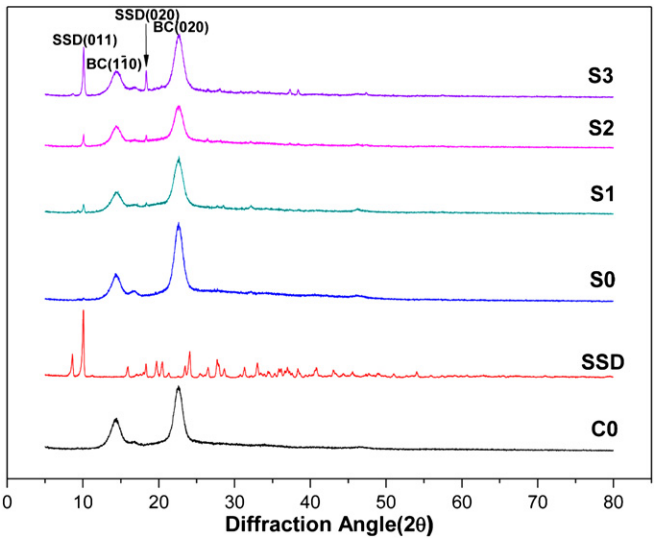

Figure 5. XRD patterns of BC (C0), SSD and SSD–BCs (sonicated for different periods of time: S0–0 min, S1–90 min, S2–120 min, S3–150 min).

surface of SSD particles and the cationic surfaces of BC which would facilitate absorption of SSD particles into the BC network. And the electrostatic attraction increased as the absolute value of BC and SSD's zeta potential increased. Moreover, high negative values of the zeta potential indicated that the strong electrostatic repulsion between particles would prevent their aggregation and thereby stabilize the nanoparticulate dispersion [43]. Zeta potential values in the range −15 to −30 mV were common for stabilized nanoparticulates [44]. For all the reasons discussed above, the favorable range of pH was selected as 6.6–11.5. In this pH range, SSD and BC owned opposite signs of charge and their absolute value was more than 20 mV, which could render sufficient electrostatic interaction between themselves and result in effective absorption and impregnation of SSD particles into the BC fibril network. Another benefit was that the high electrostatic repulsion between SSD particles due to their negative charged surface with the zeta potential less than −20 mV could prevent SSD particles from aggregating during the process of impregnation.

3.2. Impregnation conditions

Taking into account the effects of both pH value and zeta potential on the impregnation of SSD with BC studied above, an optimum range of pH was suggested as 6.6–9.0. A further experiment was performed under conditions shown in table 1. pH = 8.0 was selected since SSD particles stayed stable and the zeta potential value was low (approximately −37 mV) in this environment.

Results of SSD content in BC are shown in table 1. The SSD content increased along with the increase of sonication time of SSD particles which corresponded to the conclusions made in 3.1.1.

3.3. Structure and morphology of SSD–BC composite membranes

3.3.1. Crystal structure of SSD–BC composite membranes. Pure BC, SSD particles and SSD–BCs sonicated for different periods of time were analyzed using XRD in order to evaluate the structural evolution of the composite during sonication (figure 5). For original BC, two apparent broad peaks and one less obvious one in between were observed and located at diffraction angles of 14.8°, 16.3° and 22.6°, respectively. These broad peaks corresponded to the primary diffraction of the crystal plane such as (1 $\bar{1}$ 0), (1 1 0) and (2 0 0), attributed to the structure of well-defined cellulose I crystal [45]. For the small molecule SSD, its characteristic peaks appeared sharper and located at values of 8.8°, 10.21° and 18.49° corresponding to (0 0 2), (0 1 1) and (0 2 0) planes. For SSD–BC composites, sample S0 without being sonicated displayed only the characteristic peaks of BC with little SSD features,

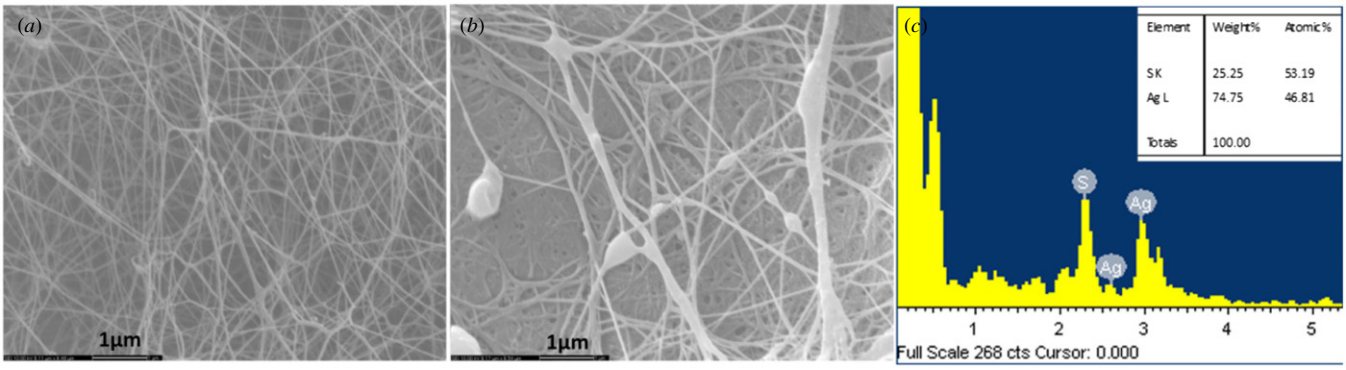

Figure 6. Scanning electron micrographs of (*a*) bacterial cellulose, (*b*) bacterial cellulose impregnated with 2% SSD (sonicated for 90 min) and (*c*) energy dispersive spectrometer (EDS) spectra of the BC-SSD sample (sonicated for 90 min).

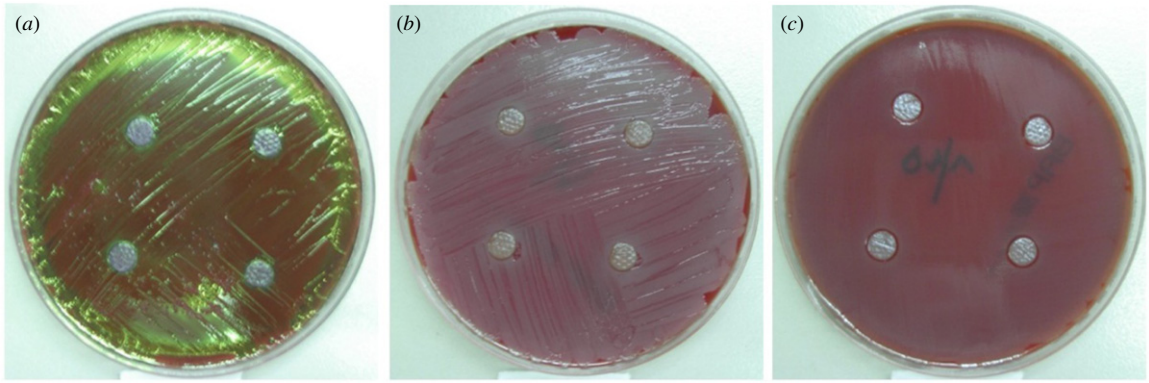

Figure 7. Representative photos of the inhibition zone of SSD-BC composites against (*a*) *Escherichia coli* (ATCC44113), (*b*) *Staphylococcus aureus* (ATCC26085) and (*c*) *Pseudomonas aeruginosa* (ATCC10211).

which indicated that original SSD hardly permeated into BC without any assistance. In contrast, the characteristic peaks of SSD at angles of 10.21° and 18.49° started to emerge in sample S1 after sonication for 90 min, and the intensity of these peaks increased in samples S2 and S3, with increasing sonication time. It is noteworthy that peak intensities rose profoundly in sample S3 after sonication for 150 min, as evidence of an increase of the load of SSD in the composites. The reason for explaining these combined diffraction peaks may be attributed to improved diffusion, permeation and absorption of SSD particles with smaller diameter, more regular and uniform shape resulting from prolonged ultrasonication, in consistence with the results discussed in section 3.1.1. Furthermore, BC's characteristic peaks remained in the composites, implying the impregnation process had little effect on the crystal structure of the cellulose microfibrils, which is highly desirable in order to preserve those outstanding properties of BC.

3.3.2. Morphology of BC and SSD–BC composite membrane. Pristine BC has a fine and dense 3D network of nanofibrils and a highly porous structure, as shown by the SEM image in figure 6(*a*), resulting in a large surface area and high porosity of the BC membrane [25]. Such a unique network plus its intrinsic hydrophilicity explains BC's outstanding properties of holding water (up to 200 times of its dry mass) and strength [25]. After the impregnation of SSD into BC's ultrafine network, the overall 3D nanofibril network of BC was well retained in spite of the formation of some thick fibrous bundles at the surface of the network after the ultrasonic process (figure 6(*b*)). Some fibrils appear to be a very thin layer with some bright particles attached, which represent the impregnated SSD particles in SSD–BC composites confirmed by EDS results. From EDS results, the S/Ag atomic ratio is approximately 1, corresponding to the SSD molecular formula result. The observation from figures 6(*b*) and (*c*) further supports the above impregnation conditions.

3.4. Antimicrobial activity of SSD–BC composite membranes

The antimicrobial activity of SSD–BC composite membranes for *P. aeruginosa, E. coli* and *S. aureus* was measured by the disc diffusion method (figure 7). The diameter of inhibition zone (DIZ) reflects a magnitude of antimicrobial ability of the microorganism. It was found that, in every test, SSD–BC composite exhibited an obvious inhibition zone against the three kinds of typical bacteria; in contrast, no inhibition zone was observed for the pure BC (figure 8). This demonstrates that antimicrobial activity is attributed to SSD particles impregnated inside BC rather than BC itself. The DIZ was also strongly affected by the sonication time. A similar trend was presented in the tests of all three kinds of bacteria in figure 8, in that the longer sonication time was applied and the larger DIZ developed. Clearly, this is directly related to increasing SSD load in the composites with

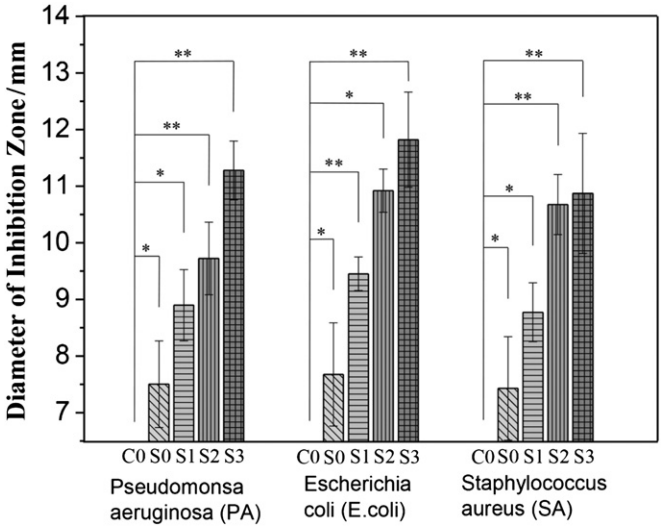

Figure 8. Diameter of inhibition zone of BC and SSD-BC (original diameter of sample was 6.5 mm). Significance: *: $P < 0.05$; **: $P < 0.01$.

increasing sonication time, in evidence of the SSD content results in table 1. Moreover, all the composite samples tested against *P. aeruginosa*, *E. coli* and *S. aureus* showed significant differences ($P < 0.05$) compared with the pure BC. The SSD–BC composites exhibited similar antibacterial effectiveness against *P. aeruginosa* and *S. aureus*. In the case of *E. coli*, the DIZ of S0, S1, S2, S3 was respectively 2%, 6%, 12% and 5% greater than that in the case of *P. aeruginosa*. In comparison with *S. aureus*, the values became 3%, 8%, 2% and 9%. Hence, based on the DIZ values against the model bacteria, the highest antimicrobial activity was demonstrated on *E. coli*.

3.5. Biocompatibility of SSD–BC composite membranes

3.5.1. Cell morphology. Epidermal cells cultured for different periods of time were stained with the Rhodamine/Nile blue and were then observed using an inverted biological microscope (figure 9). After culturing for 1 d, epidermal cells were sparsely spreaded more or less everywhere with some notable dense cell domains. Most epidermal cells had a round shape. There were no significant differences between groups. On the fourth day, the number of cells increased obviously with more rounder and larger flat epidermal cells produced, demonstrating that epidermal cell proliferation had begun. In the meantime, epidermal cells started to give rise to fibroblasts in each group, which were spindle-shaped or irregular triangular. Cell growth continued in well spread ways on the seventh day. At this stage, epidermal cells were still in round and flat shape, but fibroblast growth differed from group to group. A fibroblast fusion started to take place in $C0_7$ and $S0_7$ groups in the appearance of denser domains of spindle-shaped and irregular triangular cells distributed in the culture medium between the epidermal cells. In contrast, there were few signs of cell fusion in $S1_7$, $S2_7$ and $S3_7$ groups. Nevertheless, after culturing for ten days, more fibroblasts grew in all groups and then converged to form large areas in the culture medium. As a result, epidermal cells were gradually masked by many fibroblasts. There were no significant differences between groups.

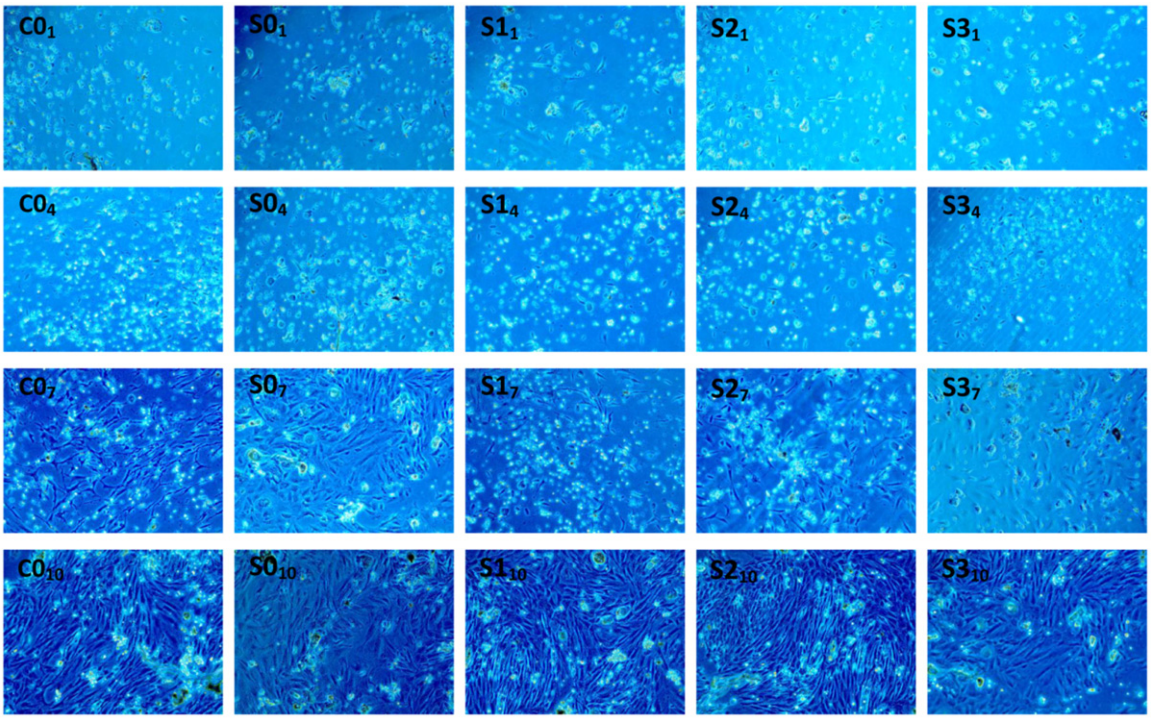

Figure 9. Epidermal cell morphology of different samples after 1 d, 4 d, 7 d and 10 d. C0: pure BC membrane; S0: SSD-BC composites (SSD sonicated for 0 min); S1: SSD-BC composites (SSD sonicated for 90 min); S2: SSD-BC composites (SSD sonicated for 120 min); S3: SSD-BC composites (SSD sonicated for 150 min). $C0_1$, $C0_4$, $C0_7$, $C0_{10}$: cell cultured for 1d, 4d, 7d and 10d of C0 sample; $S0_1$, $S0_4$, $S0_7$, $S0_{10}$: cell cultured for 1d, 4d, 7d and 10d of S0 sample; $S1_1$, $S1_4$, $S1_7$, $S1_{10}$: cell cultured for 1d, 4d, 7d and 10d of S1 sample; $S2_1$, $S2_4$, $S2_7$, $S2_{10}$: cell cultured for 1d, 4d, 7d and 10d of S2 sample; $S3_1$, $S3_4$, $S3_7$, $S3_{10}$: cell cultured for 1d, 4d, 7d and 10d of S3 sample.

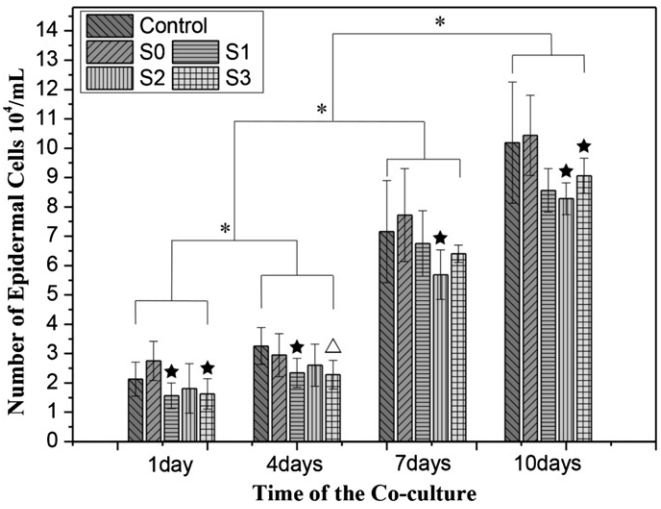

Figure 10. Epidermal cell counting results of control and SSD-BC after 1 d, 4 d, 7 d and 10 d. Significance ($P < 0.05$): Δ greater than all the others, ★ greater than control; ($P < 0.01$): * greater than the other days.

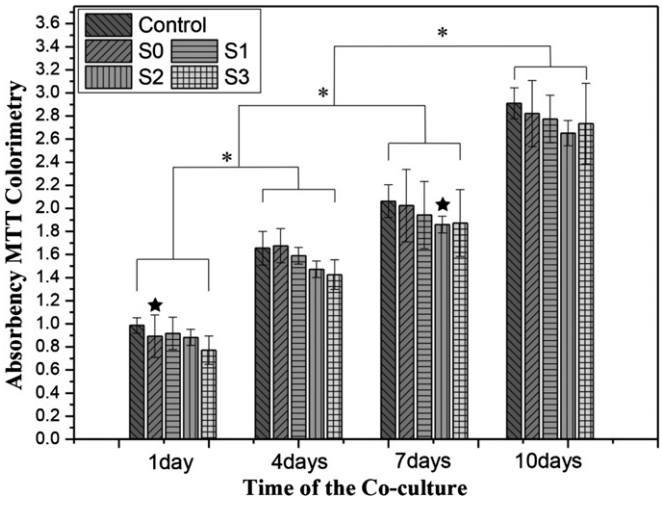

Figure 11. MTT results of control and SSD-BC composites after 1 d, 4 d, 7 d and 10 d. Significance ($P < 0.05$): ★ greater than control; ($P < 0.01$): * greater than the other days.

The observation above showed that there were no significant differences between pure BC (C0) and SSD–BC composites (S0, S1, S2 and S3), indicating SSD–BC composites possessed good biocompatibility similar to BC. The favorable environment provided by SSD–BC encouraged a small amount of fibroblasts to emerge in each group in the early days of the culturing. Regardless of the impregnation of SSD, SSD–BC composites showed low toxicity and supported the growth of epidermal cells and fibroblasts. This will be further proven by the following statistic analysis of cellular proliferation and viability of cell growth.

3.5.2 Cell count. To investigate the SSD's influence on the cellular proliferation, the hemocytometer was used to carry out the test and the results were analyzed in figure 10. Regardless of different SSD loads obtained by varying sonication time from 90 (S1) to 150 min (S3), the presence of SSD particles in the membranes decreased the proliferative capacity of cells to a certain extent, as compared with controls (figure 10). In comparison, 7 out of 16 samples of SSD–BC composites showed significant differences ($P < 0.05$). Nevertheless, the cell number of all the groups was still 75% greater than the control sample, indicating that the harmful effects of SSD–BC composites on cell proliferation were relatively low. Although the SSD–BC samples inhibited the cell growth to some degree, the number of epidermal cells increased progressively with the increase in the culture time with great significance ($P < 0.01$). This statistic measurement further quantifies the growth of epidermal cells observed in figure 9. Hence, the effects of SSD–BC composites on cellular proliferation are limited, which should encourage further investigation of SSD–BC membranes as a promising wound dressing.

3.5.3. MTT assay. The MTT data describe the relative viability of epidermal cells growing on different samples. The results analyzed in figure 11 are comparable since the same number of cells was added to all samples. The formazan absorbance indicates that the epidermal cells seeded onto the control sample (the polystyrene cell culture plate) and different membranes were able to convert MTT into a blue formazan product. It was observed that the S0 sample exhibited the best cytocompatibility among all the membranes overall. Furthermore, with increasing culture time, the viability of cells on each membrane increased significantly ($P < 0.01$), as shown in figure 11. Notably, most SSD–BC samples showed no significant differences against the control in MTT absorbance except two samples of 1d and 7d ($P < 0.05$). Therefore, it can be concluded that the addition of the SSD to BC membranes did not affect the cytocompatibility greatly, and the SSD–BC membranes have the potential to be used for antimicrobial wound dressing.

Although the biocompatibility of BC, silver and SSD have been studied extensively in the literature, the cytocompatibility of antimicrobial composites like BC–Ag, BC–benzalkonium chloride and BC–AgCl have not been reported [5, 24, 27–29]. Thus, the BC–SSD's positive effects on cells *in vitro* may shed light on future investigation.

4. Conclusions

A potential new SSD–BC wound dressing acquiring antimicrobial and biocompatible abilities has been developed and systematically studied. An ultrasonication-assisted process to produce SSD impregnated BC membranes has been developed and optimized. Sonication time of SSD particles, pH value of the environment and zeta potential of SSD or BC all have great influences on the impregnation process and thus SSD load. Sufficient sonication time (⩾90 min) and suitable pH value (between 6.6 and 9.0) assisted the formation of uniform and stable SSD particle suspension with desired particle size and negatively charged surface and therefore facilitated the diffusion, permeation and absorption of SSD through BC's 3D fibril network. In the optimized case of pH = 8.0, stable SSD particles with low negative zeta potential value (approximately −37 mV) ensured effective

impregnation of SSD with BC, meanwhile preserving its cellulose crystal structure and fibril network, proven by structure and morphology results using XRD and SEM. By applying the disc diffusion method and comparing with the BC samples, SSD–BC composite membranes showed effective antimicrobial activities against *P. aeruginosa*, *E. coli* and *S. aureus*, among which, the highest antimicrobial activity was found on *E. coli*. The favorable biocompatibility of SSD–BC was verified by MTT colorimetry and the epidermal cell counting method, along with optical microscopic images. Results indicated that the effects of SSD impregnation and load on cytocompatibility of the BC membrane were limited and acceptable. Therefore, SSD–BC membranes have been proven to be promising antimicrobial dressing for wound treatment.

Acknowledgments

This study is financially supported by National Natural Science Foundation of China Project (grant no. 51073024 and 51273021), the Royal Society-NSFC International Joint Project (grant no. 51111130207) and Beijing Municipal Science and Technology Plan Projects (no. Z111103066611005).

References

[1] Cho Lee A R, Leem H, Lee J and Park K C 2005 Reversal of silver sulfadiazine-impaired wound healing by epidermal growth factor *Biomaterials* **26** 4670–76

[2] Kennedy P, Brammah S and Wills E 2010 Biofilm and a new appraisal of burn wound sepsis *Burns* **36** 49–56

[3] Elsner J J, Berdicevsky I and Zilberman M 2011 *In vitro* microbial inhibition and cellular response to novel biodegradable composite wound dressings with controlled release of antibiotics *Acta Biomater.* **7** 325–36

[4] Ovington L G and Pierce B 2001 Wound dressings: form function feasibility and facts *Chronic Wound Care: A Clinical Sourcebook for Healthcare Professionals* ed D Krasner and G Rodeheaver *et al* (Malvern, PA: Health Management Publications Inc)

[5] Maneerung T, Tokura S and Rujiravanit R 2008 Impregnation of silver nanoparticles into bacterial cellulose for antimicrobial wound dressing *Carbohydr. Polym.* **72** 43–51

[6] Brown R M Jr, Willison J H M and Richardson C L 1976 Cellulose biosynthesis in *Acetobacter xylinum*: visualization of the site of synthesis and direct measurement of the in vivo process *Proc. Natl Acad. Sci. USA* **73** 4565–9

[7] Rambo C R, Recouvreux D O S, Carminatti C A, Pitlovanciv A K, Antônio R V and Porto L M 2008 Template assisted synthesis of porous nanofibrous cellulose membranes for tissue engineering *Mater. Sci. Eng.* C **28** 549–54

[8] Iguchi M, Yamanaka S and Budhiono A 2000 Bacterial cellulose—a masterpiece of nature's arts *J. Mater. Sci.* **35** 261–70

[9] Okiyama A, Motoki M and Yamanaka S 1992 Bacterial cellulose II: processing of the gelatinous cellulose for food materials *Food Hydrocolloids* **6** 479–87

[10] Yamanaka S, Watanabe K, Kitamura N, Iguchi M, Mitsuhashi S, Nishi Y and Uryu M 1989 The structure and mechanical properties of sheets prepared from bacterial cellulose *J. Mater. Sci.* **24** 3141–5

[11] Svensson A, Nicklasson E, Harrah T, Panilaitis B, Kaplan D L, Brittberg M and Gatenholm P 2005 Bacterial cellulose as a potential scaffold for tissue engineering of cartilage *Biomaterials* **26** 419–31

[12] Bodin A, Concaro S, Brittberg M and Gatenholm P 2007 Bacterial cellulose as a potential meniscus implant *J. Tissue Eng. Regen. Med.* **1** 406–8

[13] Fontana J D, de Souza A M, Fontana C K, Torriani I L, Moreschi J C, Gallotti B J, de Souza S J, Narcisco G P, Bichara J A and Farah L F 1990 *Acetobacter* cellulose pellicle as a temporary skin substitute *Appl. Biochem. Biotechnol.* **24–25** 253–64

[14] Novaes A B Jr, Novaes A B, Grissi M F M, Soares U N and Gabarra F 1993 Gengiflex, an alkali–cellulose membrane for GTR: histologic observations *Braz. Dent. J.* **4** 65–71

[15] Novaes A B Jr and Novaes A B 1997 Soft tissue management for primary closure in guided bone regeneration: surgical technique and case report *Int. J. Oral Maxillofac. Implants* **12** 84–7

[16] Salata L A, Craig G T and Brook I M 1995 *In-vivo* evaluation of a new membrane (Gengiflex®) for guided bone regeneration (GBR) *J. Dent. Res.* **74** 825

[17] Klemm D, Schumann D, Udhardt U and Marsch S 2001 Bacterial synthesized cellulose-artificial blood vessels for microsurgery *Prog. Polym. Sci.* **26** 1561–603

[18] Backdahl H, Helenius G, Bodin A, Nannmark U, Johansson B R, Risberg B and Gatenholm P 2006 Mechanical properties of bacterial cellulose and interactions with smooth muscle cells *Biomaterials* **27** 2141–9

[19] Backdahl H, Esguerra M, Delbro D, Risberg B and Gatenholm P 2008 Engineering microporosity in bacterial cellulose scaffolds *J. Tissue Eng. Regen. Med.* **2** 320–30

[20] Wippermann J, Schumann D, Klemm D, Kosmehl H, Salehi–Gelani S and Wahlers T 2009 Preliminary results of small arterial substitute performed with a new cylindrical biomaterial composed of bacterial cellulose *Eur. J. Vasc. Endovasc. Surg.* **37** 592–6

[21] Sokolnicki A M, Fisher R J, Harrah T P and Kaplan D L 2006 Permeability of bacterial cellulose membranes *J. Membr. Sci.* **272** 15–27

[22] Amin M C I M, Ahmad N, Halib N and Ahmad I 2012 Synthesis and characterization of thermo- and pH-responsive bacterial cellulose/acrylic acid hydrogels for drug delivery *Carbohydr. Polym.* **88** 465–73

[23] Yano H, Sugiyama J, Nakagaito A N, Nogi M, Matsuura T, Hikita M and Honda K 2005 Optically transparent composites reinforced with networks of bacterial nanofibers *Adv. Mater.* **17** 153–5

[24] Pinto R J B, Marques P A A P, Neto P C, Trindade T, Daina S and Sadocco P 2009 Antibacterial activity of nanocomposites of silver and bacterial or vegetable cellulosic fibers *Acta Biomater.* **5** 2279–89

[25] Czaja W, Krystynowicza A, Bielecki S and Malcolm Brown R Jr 2006 Microbial cellulose—the natural power to heal wounds *Biomaterials* **27** 145–51

[26] Robson M C 1997 Wound infection: a failure of wound healing caused by an imbalance of bacteria *Surg. Clin. North Am.* **77** 637–50

[27] Yang G, Xie J J, Hong F, Cao Z J and Yang X X 2012 Antimicrobial activity of silver nanoparticle impregnated bacterial cellulose membrane: effect of fermentation carbon sources of bacterial cellulose *Carbohydr. Polym.* **87** 839–45

[28] Wei B, Yang G and Hong F 2011 Preparation and evaluation of a kind of bacterial cellulose dry films with antibacterial properties *Carbohydr. Polym.* **84** 533–38

[29] Hu W L, Chen S Y, Li X, Shi S K, Shen W, Zhang X and Wang H P 2009 *In situ* synthesis of silver chloride nanoparticles into bacterial cellulose membranes *Mater. Sci. Eng.* C **29** 1216–19

[30] Kim J, Cai Z J and Chen Y 2010 Biocompatible bacterial cellulose composites for biomedical application *J. Nanotech. Eng. Med.* **1** 011006
[31] Atiyeh B S, Costagliola M, Hayek S N and Dibo S A 2007 Effect of silver on burn wound infection control and healing: review of the literature *Burns* **33** 139–48
[32] Heimbach D, Mann R and Engrav L 2002 Evaluation of the burn wound management decisions *Total Burn Care* 2nd edn (New York: Saunders)
[33] Seetharaman S, Natesan S, Stowers R S, Mullens C, Baer D G, Suggs L J and Christy R J 2011 A PEGylated fibrin-based wound dressing with antimicrobial and angiogenic activity *Acta Biomater.* **7** 2787–96
[34] Konrad D, Tsunoda M, Weber K, Corney S J and Ullmann L 2001 Effects of a topical silver sulfadiazine polyurethane dressing (Mikacure) on wound healing in experimentally infected wounds in the pig *J. Exp. Anim. Sci.* **42** 31–43
[35] Modak S M and Fox C L 1973 Binding of silver sulfadiazine to the cellular components of Pseudomonas aeruginosa *Biochem. Pharmacol.* **22** 2391–404
[36] Klasen H J 2000 A historical review of the use of silver in the treatment of burns: II. Renewed interest for silver *Burns* **26** 131–8
[37] Harrison H N 1979 Pharmacology of sulfadiazine silver. Its attachment to burned human and rat skin and studies of gastrointestinal absorption and extension *Arch. Surg.* **114** 281–5
[38] Monafo W W and West M A 1990 Current treatment recommendation for topical burn therapy *Drugs* **40** 364–73
[39] Ward R S and Saffle J R 1995 Topical agents in burn and wound care *Phys. Ther.* **75** 526–38
[40] Herruzo-Cabrera R, Gracia-Torres V, Rey-Calero J and Vizcaino-Alcaide M J 1992 Evaluation of the penetration strength, bactericidal efficacy and spectrum of action of several antimicrobial creams against isolated microorganisms in a burn centre *Burns* **18** 39–44
[41] Kuroyanagi Y, Kim E, Kenmochi M, Ui K, Kageyama H, Nakamura M, Takeda A and Shioya N 1992 A silver-sulfadiazine-impregnated synthetic wound dressing composed of poly-L-leucine spongy matrix: an evaluation of clinical cases *J. Appl. Biomater.* **3** 153–61
[42] Xu F J, Zhu Y, Chai M Y and Liu F S 2011 Comparison of ethanolamine/ethylenediamine-functionalized poly(glycidyl methacrylate) for efficient gene delivery *Acta Biomater.* **7** 3131–40
[43] Feng S and Huang G 2001 Effects of emulsifiers on the controlled release of paclitaxel (Taxol) from nanospheres of biodegradable polymers *J. Controlled Release* **71** 53–69
[44] Musumeci T, Ventura C A, Giannone I, Ruozi B, Montenegro L, Pignatello R and Puglisi G 2006 PLA/PLGA nanoparticles for sustained release of docetaxel *Int. J. Pharm.* **325** 172–9
[45] Isogai A, Usuda M, Kato T, Uryu T and Atalla R H 1989 Solid-state CP/MAS 13C NMR study of cellulose polymorphs *Macromolecules* **22** 3168–72